Article

Beyond the Toolpath: Site-Specific Melt Pool Size Control Enables Printing of Extra-Toolpath Geometry in Laser-Wire Directed Energy Deposition

Brian T. Gibson[1],*, Brad S. Richardson[1], Taylor W. Sundermann[2] and Lonnie J. Love[1]

[1] Manufacturing Demonstration Facility, Oak Ridge National Laboratory, Knoxville, TN 37932, USA
[2] University of Nebraska, Lincoln, NE 68588, USA
* Correspondence: gibsonbt@ornl.gov

Featured Application: This work applies to the production of large, complex, metallic pre-form structures in the aerospace and tool and die industries. In the aerospace industry, this technology has a potential role in the rapid production of custom, near-net shape pre-forms for machined Ti-6Al-4V components. Specifically, site-specific control enables localized control of bead geometry, which has enhanced defect mitigation capabilities and may enable local control of material properties.

Abstract: A variety of techniques have been utilized in metal additive manufacturing (AM) for melt pool size management, including modeling and feed-forward approaches. In a few cases, closed-loop control has been demonstrated.   In this research, closed-loop melt pool size control for large-scale, laser-wire based Directed Energy Deposition is demonstrated with a novel modification: site-specific changes to the controller set-point were commanded at trigger points, the locations of which were generated by the projection of a secondary geometry onto the primary 3D-printed component geometry. The present work shows that, through this technique, it is possible to print a specific geometry that occurs beyond the actual toolpath of the print head. This is denoted as an extra-toolpath geometry and is fundamentally different from other methods of generating component features in metal AM. A proof-of-principle experiment is presented in which a complex oak leaf geometry was embossed on an otherwise ordinary double-bead wall made from Ti-6Al-4V. The process is introduced and characterized primarily from a controls perspective with reports on the performance of the control system, the melt pool size response, and the resulting geometry. The implications of this capability, which extend beyond localized control of bead geometry to the potential mitigations of defects and functional grading of component properties, are discussed.

1. Introduction

Monitoring and control of metal additive manufacturing (AM) processes is the subject of intense research interest, from powder bed fusion to wire- or powder-based Directed Energy Deposition (DED). Particularly in large-scale wire-based DED, real-time sensing and control are part of the array of techniques being employed to address the primary technical challenge, which is simultaneous management of geometry, material properties, and residual stress and distortion [1]. In terms of thermal control, closed-loop melt pool size control via power modulation has proven to be an important capability; this mode of control has been demonstrated by Hu et al. in laser cladding, Hu et al. and Hofmeister et al. in laser-powder based DED, Zalameda et al. in Electron Beam Freeform Fabrication, and the present authors in laser-wire based DED [2–6]. This mode of control effactually enables control of local bead geometry and management of interlayer energy density as heat accumulates in the component during construction [6]. The degree to which thermal gradients and

heating and cooling rates are modified by this mode of control, and the subsequent impacts on solidification dynamics, microstructure, and material properties, is the subject of continuing investigation, largely on a machine- and material-specific basis.

The literature indicates that, in the research demonstrated to date, the common goal of efforts to control the melt pool size in DED has been to maintain a consistent melt pool size with a constant controller set-point. This type of control has the effect of maintaining nominal bead geometry both on an intralayer basis and throughout the printing of components, yielding global geometry control. However, the concept of site-specific modifications to deposition parameters, which are driven by additional information attached to the toolpath, is of great interest to AM researchers; after all, one of the unique benefits of AM is that it affords manufacturing flexibility in the form of shape, hierarchical, material, and functional complexity [7]. Site-specific parameter modifications can enable local bead geometry control, vary the magnitude of energy input, and induce changes to thermal gradients and rates of solidification for functionally grading the material properties of components [8]. This capability was demonstrated in Electron Beam Melting, a powder-bed AM process, with site-specific control of crystallographic grain orientation in a nickel-based superalloy, Inconel 718, which was achieved through open-loop changes to scan strategy [9].

For large-scale DED, pre-programmed, open-loop changes to primary process parameters, such as laser power, print speed, and deposition rate, are also possible. However, the mode of operation proposed here is to command site-specific modifications (e.g. melt pool size) at desired set-points under closed-loop control. In this way, a system would be capable of automatically achieving consistent property modifications in the presence of the ever-changing thermal conditions of the component under construction. Demonstrating this technology served as the motivation for this research. In this work, a proof-of-principle experiment was completed in which a laser hot-wire DED process was used to print Ti-6Al-4V components with closed-loop control of melt pool size through laser power modulation, and site-specific changes were commanded to the melt pool size at locations determined by a secondary, extra-toolpath ('extra-' denoting specific, printed geometry that occurs beyond the toolpath) geometry. The performance of the control system, melt pool size response, and resulting geometry are presented. Because this research was conducted through a public-private partnership, some details are considered protected intellectual property (IP) and have therefore not been included in the article.

2. Materials and Methods

Titanium components printed for this study were deposited in a custom, large-scale laser-hot wire DED workcell. The workcell contained a 6-axis industrial robot, wirefeeder, hot-wire system, and was supplied by two fiber-delivered diode lasers, the power from which was combined into a single fiber for 20 kW of total laser power. In addition to the laser optics, the print head contained in-axis process and thermal cameras as well as a laser line scanner. The in-axis cameras received emissions from the melt pool that were transmitted through a dichroic mirror in the laser optics. The process camera was primarily used to monitor process stability and identify process interruptions, such as an improper wire input location or unstable wirefeed behavior. The thermal camera was used to image the melt pool and generate a thermal field, which was processed to generate a melt pool definition in real-time. The generated definition of melt pool size was low-noise, which is desirable from a controls perspective, and consistently tracked with the thermal properties of the build, behavior that has been realized through an extensive research and development effort. Additional detail regarding the thermal camera, including calibration and several other melt pool measurement considerations, are available in prior work [10]. Example false-color images from the thermal camera are shown in Figure 1, along with the corresponding thresholded images that contain only that which is defined as the melt pool.

The melt pool size signal was provided to a closed-loop controller that manipulated laser power in real-time to control melt pool size. The controller was of a typical linear, feedback control architecture. While the specific control law and gain values utilized are considered protected IP, it is

95   noteworthy that the controller was tuned for set-point tracking performance. The controller
96   architecture is diagramed in Figure 2.

97
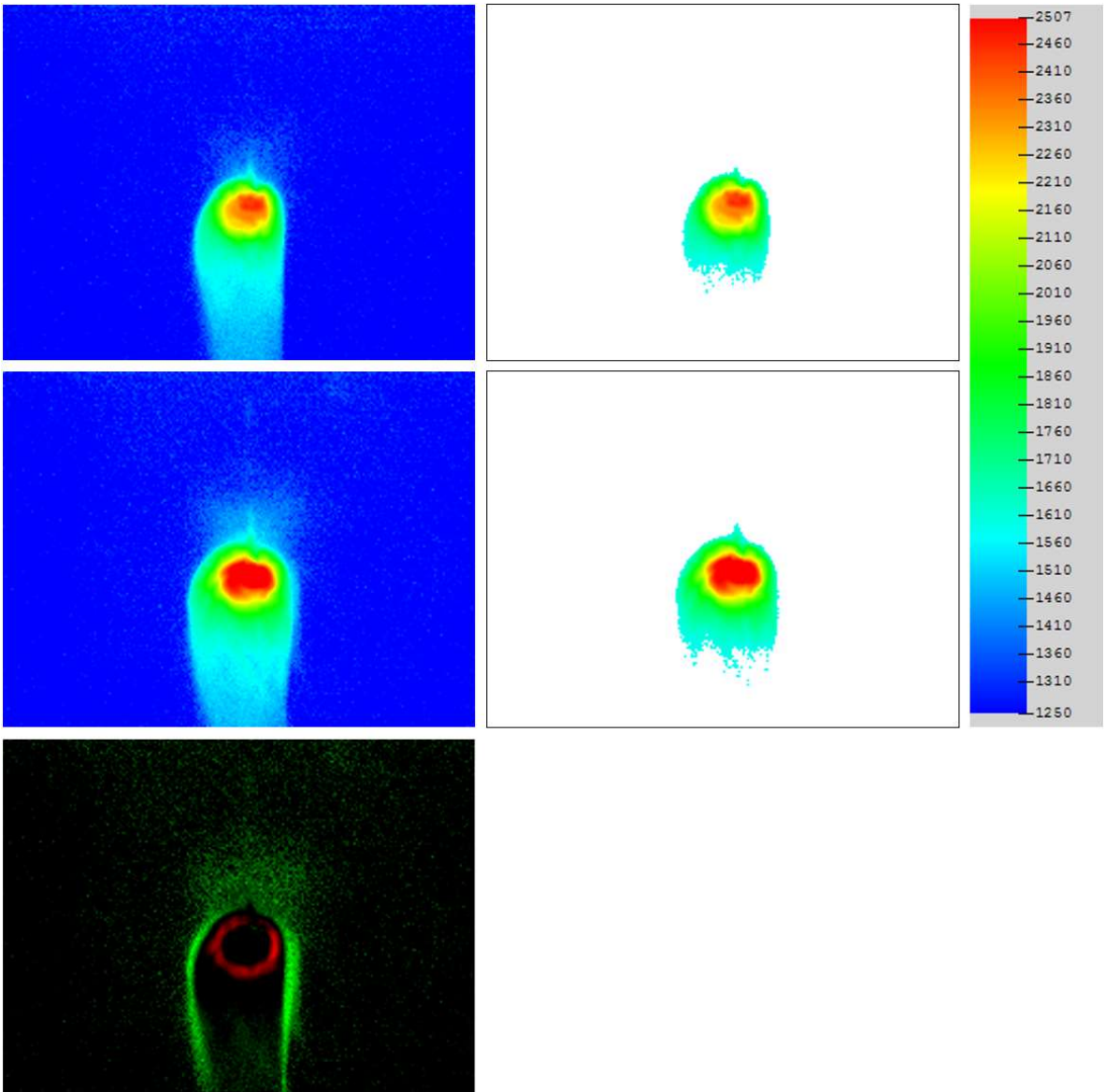
Figure 1. Thermal Camera Images of the Melt Pool; As-Collected Nominal Size (top left), Thresholded
Nominal Size (top right), As-Collected Increased Size (middle left), Thresholded Increased Size
(middle right), As-Collected Comparison (bottom left).

101

102
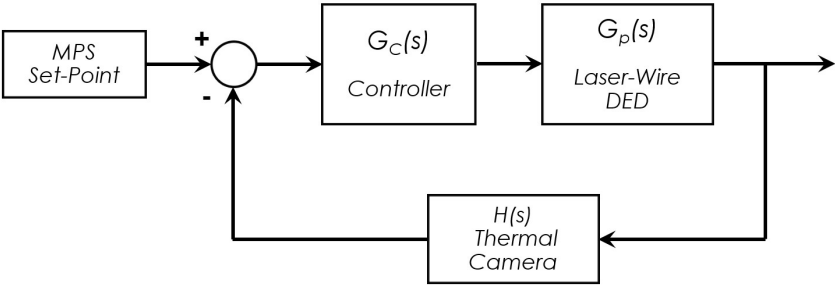
Figure 2. Closed-Loop Controller Architecture.

104   The desired melt pool size set-point was provided to the controller in pixels. While this
105 parameter would typically be maintained at a constant value throughout the printing of a component,
106 in this research it was changed at specified trigger points, the locations of which were determined by
107 a secondary geometry. In addition to laser power being continuously modulated, other process
108 variables were also subjected to manipulation through additional process control algorithms. The
109 laser line scanner on the print head was used to measure layer height, relative to the nominal ideal
110 layer height, on an interlayer basis. Deviations then drove parameter modifications on subsequent
111 layers to correct errors, a process described in ref [11]. Given that the process variables were
112 modulated over a range of values, Table 1 displays only the nominal deposition values used for the
113 test geometry.

114

Table 1. Primary Process Parameters.

Parameter	Value	Units
Delivered Laser Power	8.71	kW
Deposition Rate	2.4	kg/hr
Print Speed	8	mm/s
Layer Height	1.6	mm
Bead Stepover	9.5	mm

115

116   The feedstock used was Ti-6Al-4V wire in 1.6 mm diameter. The build plate material was also
117 Ti-6Al-4V, with a 6.35 mm (0.25 inch) thickness. Deposition rate was a function of wire feed rate, wire
118 diameter, and feedstock density (4.43 g/cm3 for Ti-6Al-4V). The delivered amount of laser power was
119 determined through a calibration process that used a power measurement device. Depositions were
120 completed in an Argon environment maintained by a tent-like enclosure that surrounded the build
121 plate and was purged prior to printing. A steady flow of Argon throughout the printing process
122 maintained Oxygen levels below 300 ppm.
123   The concept of trigger points generated by a secondary geometry is diagramed in Figure 3. The
124 primary geometry is the traditional geometry that would be input to a slicer, i.e. it is the 3D object to
125 be printed. The object is sliced into layers that are oriented with the X-Y plane, which are then filled
126 with pathing. The secondary geometry, for the purposes of this proof-of-principle experiment, was a
127 2D geometry oriented with the Y-Z plane. This is not the only representation or orientation that is
128 possible, however. Other formats may make sense for accomplishing different objectives. The
129 intersections between the layer and the secondary geometry then drive the generation of trigger
130 points, which are distances from a common edge such as the leading edge of the primary geometry,
131 which for the test geometry in this study was the starting point for the pathing for each layer. The
132 trigger points must be stored in some format that can be attached to the tool path and used by the
133 printer. For this study, the trigger points were used by the printer's control system to command step
134 changes in melt pool size; therefore, two trigger points form a complete step (up some prescribed
135 magnitude and back down to nominal size).
136   The primary geometry selected for this study was a double-bead wall, 175 mm in length and 150
137 mm in height (94 layers with a 1.6 mm layer height). The ORNL Slicer, which was developed
138 specifically for large-scale AM, was utilized. Figure 4 shows the primary geometry in the slicer
139 environment after slicing. Note that the geometry is a simple double-bead wall with two paths per
140 layer, known as skeletons, and no additional geometric detail. Beads were deposited with the front-
141 feed wire orientation, with the exception of a bead termination routine that took place at the end of
142 each bead, in which the print head reversed to deposit additional material for a prescribed distance
143 that could evolve on a per-layer basis; this routine serves as an additional measure to maintain proper
144 layer height. The reversal distance and the nominal deposition rate evolved in the termination routine
145 according to the parameters in Table 2. In addition to helping maintain layer height, the use of the
146 termination routine can also manifest as slight wall width increases that are evident in the wall
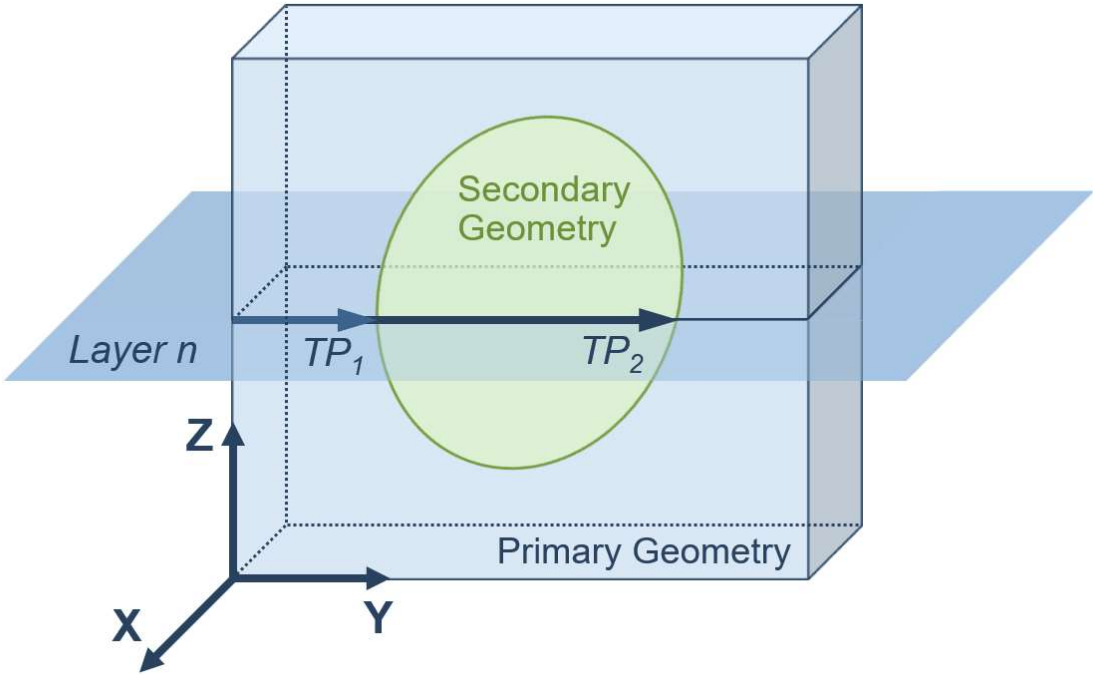147 geometry scans.

148

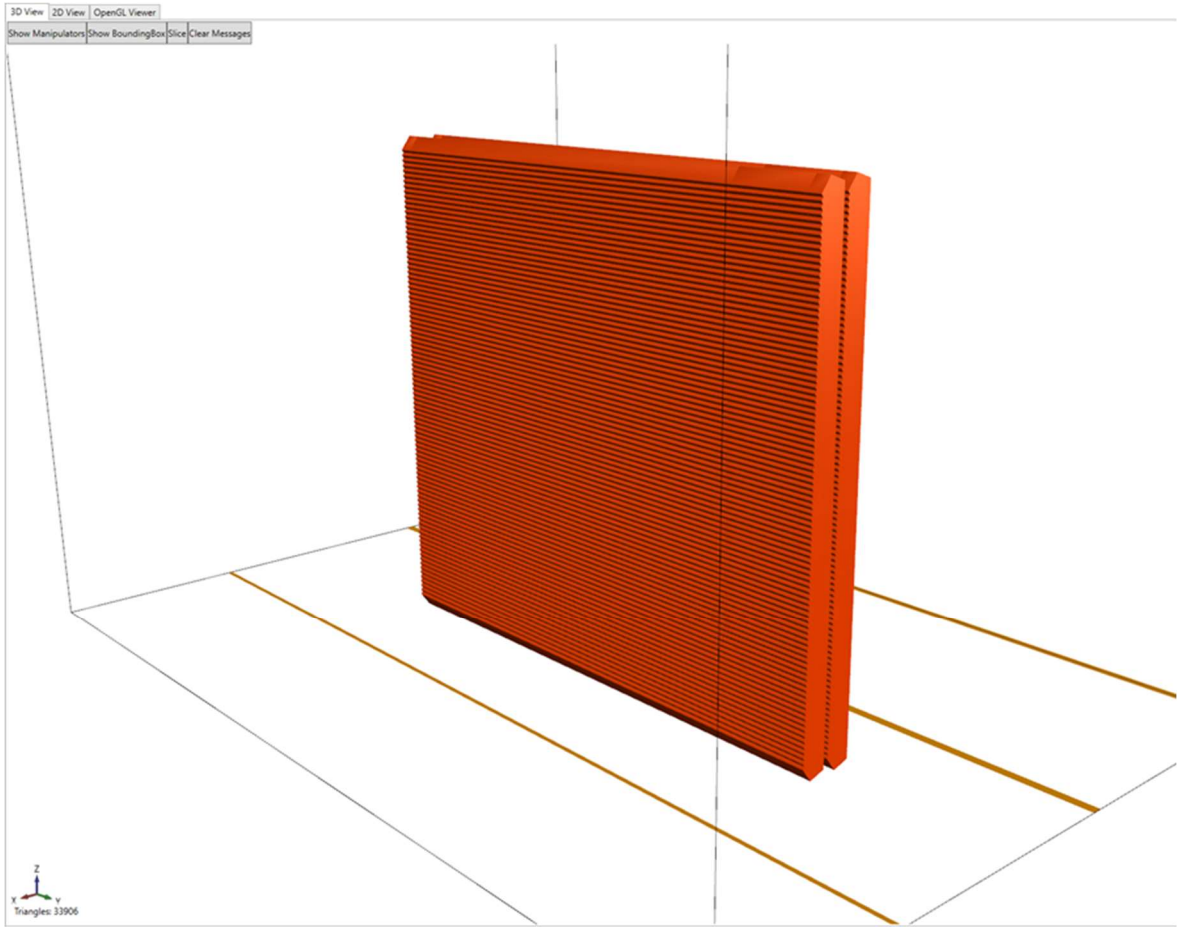149   **Figure 3**. Concept of Generating Trigger Points using a Secondary Geometry.

150

151   **Figure 4**. Double-Bead Wall in ORNL Slicer Environment.

152   **Table 2:** Bead Termination Routine Parameters.

Parameter	Value	Units
Initial Distance	10	mm
Distance Increment	1	mm
Wirefeed Increment	-2.2	%
Maximum Layer	20	

153

154   The secondary geometry selected for this study was an oak leaf. The oak leaf is a complex
155 geometry that afforded the opportunity to study the melt pool size response over a large variety of
156 step durations, a function of step distance and print speed. The oak leaf design, segmented with
157 layers, contained 139 total steps, 116 of which were of unique distances, ranging from 0.7 mm to 77.5
158 mm. It was anticipated that short step distances would be bandwidth limited, i.e. the rate of change
159 of melt pool size is limited by the physics of the melt pool, even under active closed-loop control, and
160 would provide an interesting behavioral study. Figure 5 shows the conceptual workflow for the
161 generation of the oak leaf trigger points. The workflow starts with a 2D sketch of the geometry, which
162 must be appropriately scaled and then segmented into layers using the known layer height. The
163 intersection points of the secondary geometry and the layer lines become the trigger points at which
164 the melt pool size set-point would change. For the purposes of this study, trigger points were limited
165 to a maximum of six per layer, yielding a maximum of three complete step changes in melt pool size
166 per layer. This required some filtering of fine details from the oak leaf geometry, particularly at the
167 leaf tips, but maintained the overall design and sufficient complexity. The trigger points are color
168 coded in Figure 4 to show the progression and number of triggers on a per-layer basis.

169
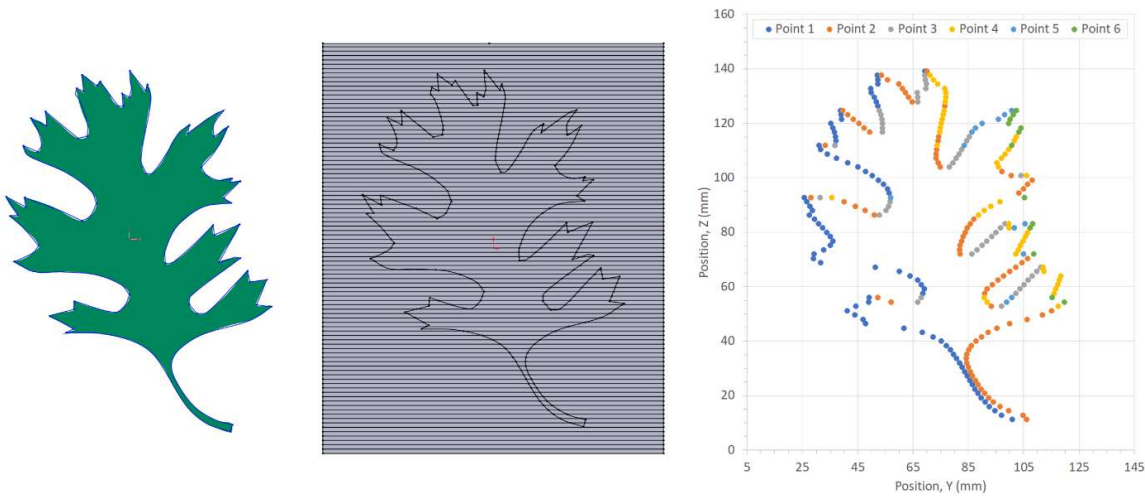
170   **Figure 5.** Generalized Workflow for Oak Leaf Trigger Point Generation; From left to right: Original
171   Sketch, Layerized Geometry, Final Trigger Points

172   Two walls were printed for this study. The first wall contained step changes in only the second
173 of two beads per layer, and the step changes commanded the melt pool size 25% higher than nominal.
174 The second wall contained step changes in both beads, and the melt pool size was commanded 37.5%
175 higher than nominal. This experimental setup allowed for a comparison of melt pool size and laser
176 power response across beads and across magnitudes of step changes. This is summarized in Table 3.
177 The nominal melt pool size was determined through testing in which deposits were made with
178 nominal parameters while only monitoring with the thermal camera; the measured melt pool size
179 then subsequently became the set-point for control. The increased melt pool size was selected to
180 produce a large increase in size while still maintaining process stability based on significant
181 experience with the deposition parameters.

182

183   **Table 3.** Test Wall Melt Pool Size Parameters.

Test Wall	Nominal Melt Pool Size (pixels)	Increased Melt Pool Size (pixels)
Wall 1		
Bead 1	2450	N/A
Bead 2	2450	3063
Wall 2		
Bead 1	2450	3369
Bead 2	2450	3369

184

The stability concern arises from the fact that if laser power increases too much, the wire feedstock can begin to transfer in droplet form, at which point it is difficult, if not impossible, to measure the melt pool size. Additionally, a command for a larger melt pool size results in an increase in laser power, which, without a corresponding increase in wirefeed rate, results in a wider and shorter bead profile. In theory, if this behavior happened repeatedly on a layer by layer basis, a height deficit could propagate and result in a major defect. The previously discussed layer height control algorithm counteracts this effect through interlayer scanning and modification of the parameters of the following layer. While the melt pool size controller and the layer height controller operate concurrently, the systems have no a priori knowledge of the other's actions, meaning that interesting interactions between the systems are certainly possible. Characterizing these interactions was not within the scope of this work, but a measurement of the final wall geometry served as an indicator of the degree to which the layer height control system accomplished its task.

The response of the melt pool size control system was characterized by examining the melt pool size and laser power behavior at select locations. The scaled melt pool size data was overlaid with robot position feedback data to generate a visualization of melt pool size for an entire half of a wall. The melt pool response time was specifically examined in the region of the oak leaf stem in wall 2, which contained the higher magnitude step changes. The stem contained a range of steps that were relatively short in duration, an ideal scenario for evaluating the minimum duration for which the melt pool set-point could actually be achieved, i.e. the process resolution. A further examination of melt pool bandwidth was not within the scope of this work, but additional information has been presented in the literature on the melt pool response for this specific laser-wire DED process [12].

Final part geometry was characterized via scanning with a FaroArm scanner, which generated virtual, 3D representations of the printed components. This allowed for a comparison of the printed geometry against an ideal representation of a flat wall with no embossed, secondary geometry. The magnitude of oak leaf embossing could be determined and compared across test cases.

3. Results

During wall printing, laser power was modulated as expected and the desired melt pool size was achieved at the set-points. Qualitative evidence of this is available in Figure 1, which shows thermal camera images of the melt pool from bead 1 of layer 35 in Wall 2. Images of high and low melt pool size set-points are shown in both the as-collected and thresholded conditions. Additionally, a comparison of the as-collected images is shown via a subtraction of RGB values in which the melt pool size difference between the high and low cases manifests as a bright green region against a field of black.

The melt pool size data from an entire half of a wall was overlaid with the corresponding tool path, i.e. feedback position data from the print head, *to provide* a high-level confirmation that the desired site-specific changes in melt pool size were achieved. Bead 1 of Wall 2 was selected for this visualization, and the result is shown in Figure 6. The melt pool size was scaled such that magnitude increases would nicely show the secondary geometry. This was accomplished by subtracting the nominal melt pool size (2450 pixels) and scaling by a factor of 10-3; the scaled value was then added to the print head Z position on a point-by-point basis. The oak leaf is clearly visible in the overlaid melt pool size data.
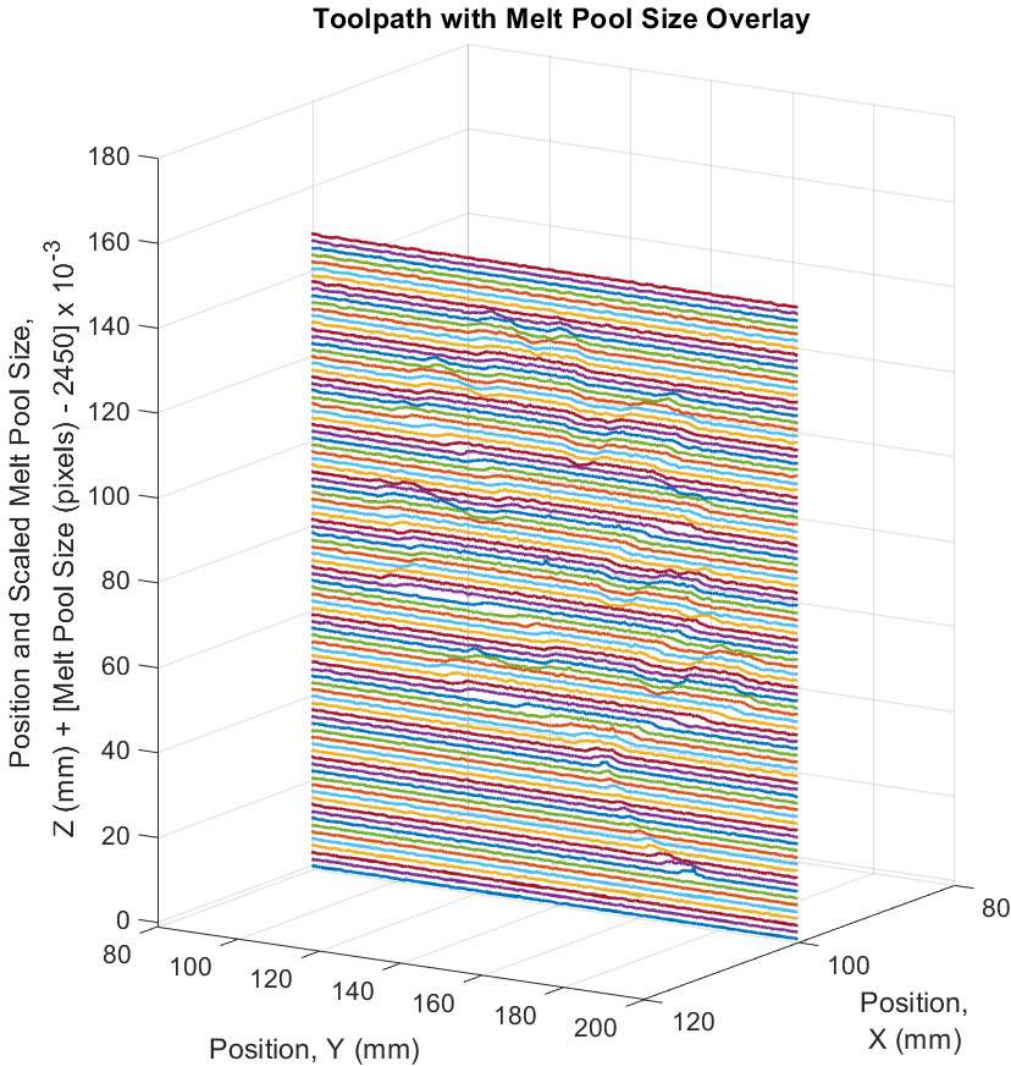
Figure 6. Toolpath with Melt Pool Size Overlay for Bead 1 of Wall 2

3.1 Laser power modulation

For a more detailed look at laser power modulation, Figure 7 displays laser power data and the melt pool size response for both beads of layer 35 for each wall. Layer 35 was selected because it contained the maximum of three step changes, and each was sufficiently long to allow the system to achieve the desired melt pool size at set-points. In Wall 1, bead 1 did not contain any site-specific step changes. Figure 7 shows that the melt pool was controlled at the nominal size (2450 pixels) throughout the bead. Some increased error is evident as the print head entered the bead termination routine (at ~24 seconds on the figure), at which point laser power was significantly modulated to control melt pool size in a highly transient thermal condition that tested the disturbance rejection capabilities of the controller, rather than set-point tracking performance. In bead 2, three step changes were present, and laser power modulated over a range of approximately 1.5 - 2 kW to achieve the higher melt pool size of 3063 pixels. It is noteworthy that the laser power required to achieve the nominal melt pool size was lower for bead 2, compared to bead 1, by approximately 0.5 - 1 kW. This result is not unexpected, in that the residual heat present in the wall after the deposition of bead 1 contributes to the deposition of bead 2, in what can be thought of as a secondary heating or insulating effect; the inter-bead time, or the duration from laser-off of bead 1 to laser-on of bead 2, was only 16 seconds. After the deposition of bead 2, however, there was a longer cooling time before the deposition of bead 1 of the subsequent layer; the interlayer time, which included the built height scan, was 89 seconds.

Figure 7. Laser Power and Melt Pool Size Response for Layer 35

In Wall 2, both beads contained site-specific step changes in melt pool size. The secondary geometry was shifted +10 mm in the Y-axis for Wall 2 to better position the leaf within the wall; this is evident as a slight shift in time of the step changes for Wall 2 compared to Wall 1. The laser power magnitude required to achieve the nominal melt pool size in Wall 2 was remarkably similar to that of Wall 1, and again, bead 2 laser power trended lower than bead 1 laser power. Where differences arise are in the step changes. Larger modulations in laser power, on the order of 2 - 3 kW, were required to achieve the increased melt pool size. Interestingly, the largest and most distinct difference between bead 1 and bead 2 laser power occurred at the two inter-step returns to nominal melt pool size, at which point bead 2 laser power was approximately 1 kW lower than bead 1. It is believed that

258   the residual heat contributed to the larger reductions in laser power that were required to return the
259   melt pool to the nominal size.

260   *3.2 Melt pool size response*

261   For a deeper dive on melt pool size response, an examination of the leaf stem region, which
262   contained a range of steps that were relatively short in duration, was conducted. Wall 2 was selected
263   for this analysis, due to its larger magnitude step changes. Specifically, layers 9 - 25, which contained
264   single step changes in the leaf stem, were examined. Figure 8 displays the melt pool response time
265   comparison for select layers in this range. Curves were temporally aligned using the rising edge of
266   the melt pool size signal to allow for direct comparisons among step durations. It was found that 2.7
267   mm, the step distance of layer 21, was the minimum step distance for which the higher melt pool size
268   set-point (3369 pixels) could be achieved. Step distances shorter than this were characterized by melt
269   pool size responses that did not attain the higher set-point; one such example is shown in Figure 7.
270   For the combination of primary process parameters used to print these walls, 2.7 mm would be
271   considered the extra-toolpath feature resolution for which full embossing could be achieved. The 2.7
272   mm step distance, in combination with an 8 mm/s print speed and a 919 pixel step magnitude,
273   corresponds to a 37 msec per 100 pixel rise time, which is remarkably similar to that which has been
274   documented in prior work on this laser-wire DED process [6]. In all, there were 18 steps shorter than
275   2.7 mm in the oak leaf design, with 7 of those located in the leaf stem.

276
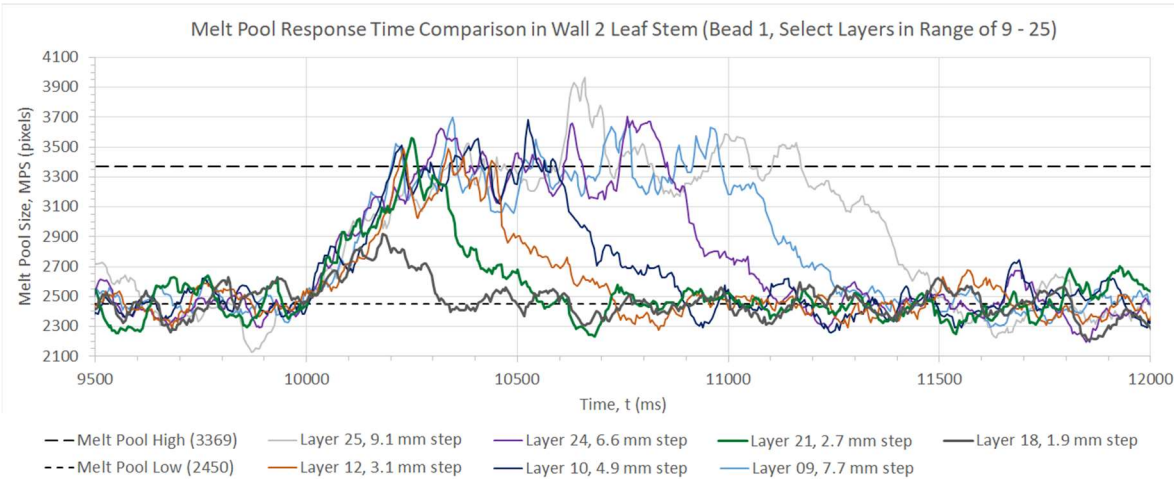
277   **Figure 8.** Melt Pool Response Time Comparison for Wall 2 Leaf Stem; Bead 1, Select Layers in the
278   Range of 9 - 25

279   *3.3 Extra-toolpath geometry*

280   Scans of the wall geometries revealed the embossed, or extra-toolpath, geometry achieved
281   through site-specific melt pool size control. Thickness color maps are shown for both sides of both
282   Walls 1 and 2 in Figure 9. The thickness maps were generated by comparing the scanned, as-printed
283   geometry with that of a flat reference wall, like that used for slicing purposes; the thickness
284   magnitude represented by the color scale is the difference between the two geometries. Relative
285   positioning of the reference wall and the scanned geometry in the inspection software led to some
286   differences in the color scale from case to case. Because of this, a white reference marker was inserted
287   into the color scale at the position believed to represent the average steady-state wall surface outside
288   of the oak leaf. Embossing measurements could then be made in comparison to the thickness
289   magnitude of this white reference marker on a case-by-case basis.
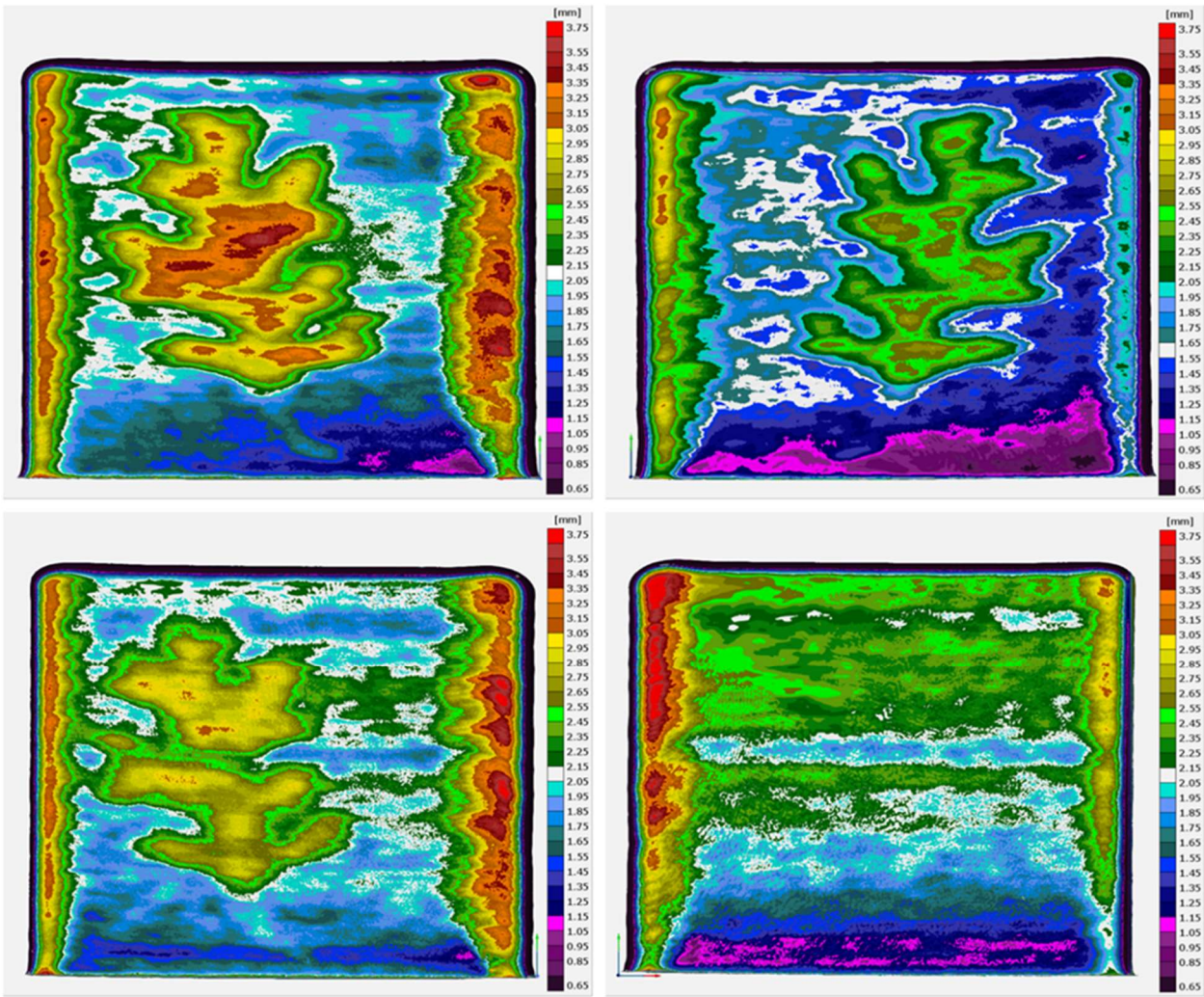
Figure 9. Wall Geometry Scans; Wall 2, Side 2 (top left), Wall 2, Side 1 (top right), Wall 1, Side 2 (bottom left), Wall 1, Side 1 (bottom right)

Wall 1, side 1 did not contain site-specific changes to the melt pool size set-point; instead, it provides a nominal reference in which some thickness variation is evident from the bottom to the top of the wall. Increases in thickness at the bead initiation and termination regions are evident and were expected. Examining the oak leaf, the maximum embossing achieved on Wall 1, side 2 was 1 mm. The maximum embossing of the oak leaf achieved on Wall 2 was 1.2 mm on side 1 and 1.5 mm on side 2. The maximum of 1.5 mm corresponds to 7.2% of the total wall thickness of 20.7 mm. The total through-thickness, from the combination of both sides 1 and 2 (because the oak leaves are mirror images of each other on Wall 2), was 2.7 mm, or 13% of total wall thickness. The leaf stem is more readily discernable on Wall 2, although its prominence is still reduced due to the previously discussed melt pool size response time and resolution limitations.

Finally, Figure 10 shows photographs of side 2 of Wall 2 in both the as-printed condition and after heat treatment. Both walls were subjected to a post-print stress-relief (720° C for t > 2 hours or 650° C for t > 2.5 hours for Ti-6Al-4V). The heat treatment process removed surface oxides (coloration) from the walls and gave a uniform appearance. The extra-toolpath geometry is clearly visible on the side of the wall.
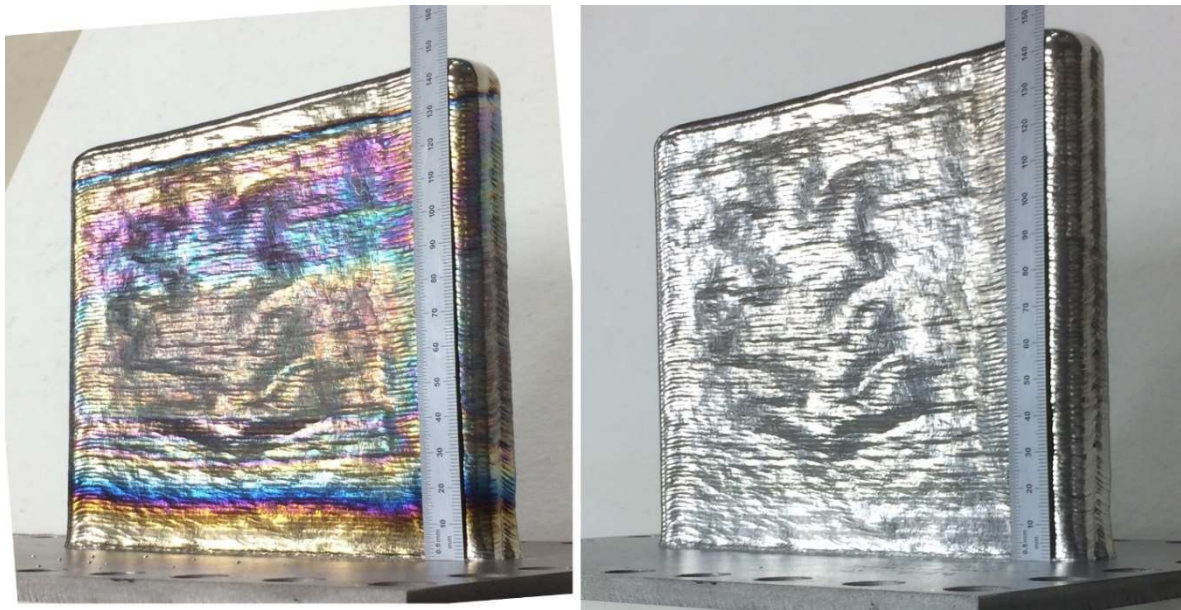
308
309   **Figure 10.** Photographs of Wall 2, Side 2; As-Printed (left), After Heat Treatment (right)

310   **4. Discussion**

311   In this work, a closed-loop, site-specific control of melt pool size was successfully utilized to
312   impart local process changes and print an extra-toolpath geometry, i.e. a geometry that occurs beyond
313   the toolpath. The embossing resolution of the extra-toolpath geometry was dependent upon the melt
314   pool size response time and the print speed. The ability of this technique to control local bead
315   geometry has interesting implications, particularly for a large-scale AM process like laser-wire DED,
316   which requires a different set of design rules than the majority of AM processes and has traditionally
317   been limited to lower resolution of component details [13, 14]. It is anticipated that the technique
318   can be used in the near future for volumetric defect mitigation in toolpaths where local overlap of
319   adjacent beads is inadequate.The capability to emboss specific, secondary geometry means that part
320   identification features, such as a serial number or QR code, could be permanently added to
321   components during the printing process. The prospect of printing single toolpath walls with varying
322   wall widths is also attractive from a post-print machining perspective, in that, when machining thin-
323   walled structures, pre-forms ideally contain integrated structural support such as thicker sections
324   that buttress and support adjacent thinner sections during the machining process.

325   An important aspect of the process demonstrated here is the closed-loop nature of the process.
326   While it would certainly be possible to pre-program open-loop, site-specific modifications to process
327   parameters in laser-wire DED, a closed-loop system ensures that variables, like melt pool size, are
328   controlled regardless of the thermal properties of the component under construction. This was
329   evident in the laser power magnitude variance between beads 1 and 2 of the walls in this study.   A
330   model-referenced feed-forward approach would be an improvement over feed-forward alone, but
331   there are certain things that are difficult to model, like unexpected print interruptions, which can
332   happen at any time and have varying durations.

333   Another method that could be used to emboss secondary geometry would be to actually make
334   the secondary geometry part of the primary toolpath, in that the sliced 3D object would contain the
335   geometry to be embossed, and the toolpath would joggle laterally while nominal process parameters
336   are maintained to create the embossing.   The issue associated with this method is that toolpath turns
337   generally induce print head velocity reductions, which can be a challenge to handle from a process
338   stability perspective, particularly when they are sharp turns, like those likely associated with
339   secondary geometry embossing. Additionally, the small, localized nature of the toolpath joggles may
340   induce print system vibrations that are undesirable.

341   The technique presented here is a fundamentally unique way of 3D printing a geometry, and
342   accordingly, an area in which there is much room for advancement is process planning and

automation, i.e. slicing and generation of what may otherwise be known as support code. The challenge in slicing is using the projection of the secondary geometry onto the primary toolpath to generate additional information that is attached to the toolpath and used to make site-specific adjustments to process parameters, e.g. melt pool size. The embossing resolution and the ability to deal with irregularities such as singularities (locations at which the layer intersects the secondary geometry at only a single point) must be built into the capabilities of the slicer. An additional challenge is in realizing the format by which additional information is attached to the toolpath. Generally, this is an area of great interest to AM researchers and may induce the rise of new forms of metadata for g-code based systems, or more widespread adoption of fully voxel-based approaches. Software support and automation of this technique open the door for more advanced capabilities, with the potential for site-specific ramp changes, multiple parameter magnitudes, and the generation of detailed texture within the realm of possibilities.

Immediate future work will focus on process planning and automation as well as the aspect of local property control. The impact of site-specific melt pool size control on thermal gradients, cooling rate, solidification dynamics, and the resulting microstructure and mechanical properties was not characterized and is not within the scope of this work, but it is of great interest due to the potential for local property control with an eye toward functionally grading components in accordance with the demands of their applications. Future investigations will seek to answer the question of the degree to which local properties can be influenced using this technique for site-specific control of melt pool size.

References

1. Babu, S.S.; Love, L.J.; Dehoff, R.R.; Peter, W.; Watkins, T.R.; Pannala, S. Additive manufacturing of materials: Opportunities and challenges. *MRS Bull.* **2015**, Volume 40, No 12, pp. 1154 - 1161.

2. Hu, D.; Mei, H.; Tao, G.; Kovacevic, R. Closed loop control of 3d laser cladding based on infrared sensing. *Proc. Solid Freeform Fab. Symp.* **2001**, pp. 129 - 137.

3. Hu, D.; Kovacevic, R. Modelling and measuring the thermal behavior of the molten pool in closed-loop controlled laser-based additive manufacturing. *Proc. Inst. Mech. Eng., Part B: J. Eng. Manuf.* **2003**, Vol. 217, pp. 441 – 452.

4. Hofmeister, W.H.; MacCallum, D.O.; Knorovsky, G.A. Video monitoring and control of the LENS process. In Proceedings of the 9th International Conference of Computer Technology in Welding, Detroit, MI, USA, Sept. 28 – 30, 1999.

5. Zalameda, J.M.; Burke, E.R.; Hafley, R.A.; Taminger, K.M.B.; Domack, C.S.; Brewer, A.; Martin, R.E. Thermal imaging for assessment of Electron-Beam Freeform Fabrication (EBF3) additive manufacturing deposits. *Proc. SPIE Thermosense: Thermal Infrared Appl. XXXV* **2013,** Volume 8705.

6. Gibson, B.T.; Bandari, Y.K.; Richardson, B.S.; Henry, W.C.; Vetland, E.J.; Sundermann, T.W.; Love, L.J. Melt pool size control through multiple closed-loop modalities in laser-wire directed energy deposition of Ti-6Al-4V. Under review.

7. Gibson, I.; Rosen, D.; Stucker, B. Additive manufacturing technologies: 3D Printing, rapid prototyping, and direct digital manufacturing. 2nd ed., Springer Link, 2015.

394 8.   Lee, Y.S.; Kirka, M.M.; Dinwiddie, R.B.; Raghavan, N.; Turner, J.; Dehoff, R.R.; Babu, S.S. Role of scan
395   strategies on thermal gradient and solidification rate in electron beam powder bed fusion. *Addit. Manuf.*
396   **2018**, Volume 22, pp. 516 - 527.
397 9.   Dehoff, R.R.; Kirka, M.M.; Sames, W.J.; Bilheux, H.; Tremsin, A.S.; Lowe, L.E.; Babu, S.S. Site-specific control
398   of crystallographic grain orientation through electron beam additive manufacturing. *J. Mater. Sci. Technol.*
399   **2015**, Volume 31, No 8, pp. 931 - 938.
400 10. Gibson, B.T.; Bandari, Y.K.; Richardson, B.S.; Roschli, A.C.; Post, B.K.; Borish, M.C.; Thornton, A.; Henry,
401   W.C.; Lamsey, M.; Love, L.J. Melt pool monitoring for control and data analytics in large-scale metal
402   additive manufacturing. *Proc. Solid Freeform Fab. Symp.* **2019**, pp. 1 - 18.
403 11. Borish, M.; Post, B.K.; Roschli, A.; Chesser, P.C.; Love, L.J.; Gaul, K.T. Defect identification and mitigation
404   via visual inspection in large-scale additive manufacturing. *JOM* **2019**, Volume 71, No 3, pp. 893 - 899.
405 12. Bristow, D. Melt pool measures and effective sensor bandwidth for direct energy deposition. In
406   Proceedings of International Solid Freeform Fabrication Symposium, Austin, TX, USA, Aug. 12 -14, 2019.
407 13. Greer, C.; Nycz, A.; Noakes, M.; Richardson, B.S.; Post, B.K.; Kurfess, T.; Love, L.J. Introduction to the
408   design rules for Metal Big Area Additive Manufacturing. *Addit. Manuf.* **2019**, Volume 27, pp. 159 - 166.
409 14. Roschli, A.; Gaul, K.T.; Boulger, A.M.; Post, B.K.; Chesser, P.C.; Love, L.J.; Blue, F.; Borish, M. Designing
410   for Big Area Additive Manufacturing. *Addit. Manuf.* **2019**, Volume 25, pp. 275 - 285.